The Journal of Immunology

RESEARCH ARTICLE | JANUARY 01 2022

Divergent Genetic Regulation of Nitric Oxide Production between C57BL/6J and Wild-Derived PWD/PhJ Mice Controls Postactivation Mitochondrial Metabolism, Cell Survival, and Bacterial Resistance in Dendritic Cells

Julia P. Snyder; ... et. al

J Immunol (2022) 208 (1): 97–109.
https://doi.org/10.4049/jimmunol.2100375

Divergent Genetic Regulation of Nitric Oxide Production between C57BL/6J and Wild-Derived PWD/PhJ Mice Controls Postactivation Mitochondrial Metabolism, Cell Survival, and Bacterial Resistance in Dendritic Cells

Julia P. Snyder,[*,†] Soyeon K. Gullickson,[*,†] Roxana del Rio-Guerra,[‡] Andrea Sweezy,[§] Bay Vagher,[*,†] Tyler C. Hogan,[†] Karolyn G. Lahue,[†] Julie A. Reisz,[¶] Angelo D'Alessandro,[¶] Dimitry N. Krementsov,[*,†,1] and Eyal Amiel[*,†,1]

Dendritic cell (DC) activation is characterized by sustained commitment to glycolysis that is a requirement for survival in DC subsets that express inducible NO synthase (*Nos2*) due to NO-mediated inhibition of mitochondrial respiration. This phenomenon primarily has been studied in DCs from the classic laboratory inbred mouse strain C57BL/6J (B6) mice, where DCs experience a loss of mitochondrial function due to NO accumulation. To assess the conservation of NO-driven metabolic regulation in DCs, we compared B6 mice to the wild-derived genetically divergent PWD/PhJ (PWD) strain. We show preserved mitochondrial respiration and enhanced postactivation survival due to attenuated NO production in LPS-stimulated PWD DCs phenocopying human monocyte-derived DCs. To genetically map this phenotype, we used a congenic mouse strain (B6.PWD-Chr11.2) that carries a PWD-derived portion of chromosome 11, including *Nos2*, on a B6 background. B6.PWD-Chr11.2 DCs show preserved mitochondrial function and produce lower NO levels than B6 DCs. We demonstrate that activated B6.PWD-Chr11.2 DCs maintain mitochondrial respiration and TCA cycle carbon flux, compared with B6 DCs. However, reduced NO production by the PWD *Nos2* allele results in impaired cellular control of *Listeria monocytogenes* replication. These studies establish a natural genetic model for restrained endogenous NO production to investigate the contribution of NO in regulating the interplay between DC metabolism and immune function. These findings suggest that reported differences between human and murine DCs may be an artifact of the limited genetic diversity of the mouse models used, underscoring the need for mouse genetic diversity in immunology research. ***The Journal of Immunology*****, 2022, 208: 97–109.**

Dendritic cells (DCs) are innate immune cells that perform complex effector functions, including phagocytosis of pathogens, Ag presentation to lymphocytes, and the production and release of inflammatory cytokines and chemokines (1–5). Metabolic reprogramming has been characterized during the activation of immune cells from both lymphocyte and myeloid lineages (6–8), in which a common feature of metabolic changes in activated immune cells is the adoption of aerobic glycolysis to support demanding biosynthetic processes such as cell proliferation and specific immune effector functions (9–13). In accordance with this, DCs exhibit an intrinsic requirement for the upregulation of aerobic glycolysis metabolism to support survival and effector functions following TLR stimulation (10–12, 14, 15). The TLR-mediated metabolic shift to increased glycolysis occurs in two distinct phases. First, DCs experience a TLR-driven "glycolytic burst" mediated by the TBK1/IKKε signaling pathway (10), which is, second, followed by a sustained phase of glycolytic metabolism that is contingent upon mTOR/HIF1α–dependent NO production (11, 15). mTOR/HIF1α signaling promotes sustained commitment to glycolysis through the induction of inducible NO synthase (iNOS; gene *Nos2*) and by the HIF1α-mediated transcriptional upregulation of key glycolytic genes (10–12).

mTOR-dependent HIF1α activity drives iNOS expression in TLR-activated DCs, leading to detectable iNOS protein expression as early as 6–8 hours following DC activation (16, 17). The long-term metabolic commitment to glycolysis in DCs is due largely to the inhibition of mitochondrial respiration by NO. NO-mediated suppression of DC mitochondrial activity and oxidative phosphorylation (11, 15) is

*Cell, Molecular, and Biomedical Sciences Program, University of Vermont, Burlington, VT; †Department of Biomedical and Health Sciences, College of Nursing and Health Sciences, University of Vermont, Burlington, VT; ‡Flow Cytometry and Cell Sorting Facility, Larner College of Medicine, University of Vermont, Burlington, VT; §Undergraduate Student Research, University of Vermont, Burlington, VT; and ¶Department of Biochemistry and Molecular Genetics, University of Colorado, Aurora, CO

[1]Cosenior authors, contributed equally to this work.

ORCIDs: 0000-0002-0759-6332 (S.K.G.); 0000-0003-3822-116X (B.V.); 0000-0003-4718-0726 (T.C.H.); 0000-0002-2258-6490 (A.D.); 0000-0003-2709-7466 (D.N.K.).

Received for publication April 20, 2021. Accepted for publication October 4, 2021.

This work was supported by the National Institutes of Health (NIH), National Institute of Allergy and Infectious Diseases (P30GM118228, 1R21AI135385-01A, T32AI055402-15, and R21 AI145306), the NIH, National Institute of Neurological Disorders and Stroke (R01 NS097596), and the National Multiple Sclerosis Society (RG-1901-33309).

Address correspondence and reprint requests to Prof. Eyal Amiel, University of Vermont, 106 Carrigan Drive, Burlington, VT 05405. E-mail address: Eyal.Amiel@med.uvm.edu

The online version of this article contains supplemental material.

Abbreviations used in this article: 11.2, B6.PWD-Chr11.2; ATCC, American Type Culture Collection; B6, C57BL/6J; dbSNP, single nucleotide polymorphism database; DC, dendritic cell; F1-11.2, 11.2.iNOS-KO.F1; F1-B6, B6.iNOS-KO.F1; 1% FBS, PBS containing 1% FBS; iNOS, inducible NO synthase; iNOS-KO, iNOS-deficient B6.129P2-*Nos2*^{tm1Lau}/J; L_{10}, 10 ng/ml LPS; L_{100}, 100 ng/ml LPS; moDC, monocyte-derived DC; MOI, multiplicity of infection; MS, mass spectrometry; OCR, oxygen consumption rate; PWD, PWD/PhJ; PWK, PWK/PhJ; RT-qPCR, quantitative RT-PCR; SEITU, *S*-ethyl-isothiourea; SNP, single nucleotide polymorphism; UHPLC, ultra-high-performance liquid chromatography.

thought to act through reversible inhibition of mitochondrial cytochrome C oxidase activity (18, 19). Sustained suppression of mitochondrial respiration by NO has been well documented (11, 15, 19), and iNOS inhibitors are able to rescue the mitochondrial defect in real time, suggesting that the impact on respiration is not a function of permanent cellular or mitochondrial damage (11). The net result of NO production in DCs is the near-complete loss of mitochondrial function and the associated process of oxidative phosphorylation. The functional consequence of this mitochondrial inhibition is the requirement for a sustained commitment to glycolysis in these cells to meet both their bioenergetic (ATP production) and biosynthetic demands (10, 14, 20). Although glycolysis can extend the lifespan of DCs in the face of altered mitochondrial activity, the lifespan of these cells is still largely regulated by their NO production (11, 15, 17).

In humans, polymorphisms in *NOS2* have been associated with differential outcomes in various infectious diseases, including tuberculosis, malaria, and septic shock, although there is conflicting evidence as to whether outcomes are mediated by specific allelic variants (21–25). A subset of DCs, dubbed TNF/iNOS–producing DCs, are critically important for the clearance of *Listeria monocytogenes* via NO production, as TNF/iNOS–producing DC-deficient mice experience uncontrolled bacterial replication and die of the infection (26, 27). The balance between the microbicidal function of NO and its self-toxic effects is particularly relevant in bacterial infections, such as *L. monocytogenes*, as unrestrained NO production results in tissue damage, necrosis, and disease progression (28, 29), underscoring the importance of careful regulation of NO production. In light of this, we hypothesize that strong evolutionary pressures exist to regulate iNOS induction so that the benefit of pathogen clearance is balanced with the cost of host cell damage, and we have employed a model in this study to examine the parameters of this balance more carefully.

To date, much of our understanding of NO-mediated DC regulation comes from studies that have been carried out exclusively in the C57BL/6J (B6) mouse strain and assumed to be characteristic of the mouse species. It has been well-noted that in vitro–differentiated B6 myeloid cells produce NO more readily than comparable human cell cultures (reviewed in 30). However, the B6 mouse represents a single genotype that resulted from >100 years of artificial selection in the laboratory and thus has not been subject to environmental selective pressure. To better mimic the immense genetic diversity in human populations, we and others have recently incorporated so-called wild-derived mice into immunology research (31–36). In the current study, we used the wild-derived PWD/PhJ (PWD) strain (37) to test the hypothesis that induction of mitochondrial-toxic levels of NO is a universal feature of activated murine DCs. Our results demonstrate highly attenuated NO production in activated DCs from PWD mice, with completely preserved mitochondrial function. To address whether this differential NO regulation is a function of intrinsic genetic differences at the *Nos2* locus, we used an additional genetic tool, the subconsomic/congenic mouse strain B6.PWD-Chr11.2 (henceforth called the "11.2" strain), which carries a PWD-derived interval on chromosome 11 containing the *Nos2* gene on a B6 background (Supplemental Fig. 1A), that mostly recapitulated the NO/mitochondrial phenotype of PWD DCs. In 11.2 mice, we find that low NO production results in intact mitochondrial respiration and enhanced postactivation DC survival but at the cost of impaired control of bacterial replication. Furthermore, metabolite tracing reveals that TCA cycle flux is modulated by NO, even at doses that do not fully inhibit respiration, highlighting the fact that NO production modulates immune cell metabolism, even at low concentrations. These data provide insights into iNOS-mediated control of DC metabolism, with the potential to inform our understanding of the human context, in which immune cell production of NO is more regulated than in murine counterparts. Whereas the importance of NO production in modulating DC activation has been established in recent years (11, 15, 17, 38), this work defines a model to understand how natural genetic variation regulates NO-dependent metabolic switches that have not previously been described. These studies represent a more physiologically relevant understanding of the complexity of DC-dependent inflammatory processes and the impact of NO production on the metabolic underpinnings associated with DC activation.

Materials and Methods

Mice

The following mouse strains were used: B6 (stock no. 000664; The Jackson Laboratory), C57BL/6J-Chr 11.2$^{PWD/Ph}$/ForeJ (stock no. 005998; The Jackson Laboratory), PWD (stock no. 004660; The Jackson Laboratory), and iNOS-deficient B6.129P2-*Nos2*^{tm1Lau}/J (iNOS-KO; stock no. 002609; The Jackson Laboratory), all purchased from The Jackson Laboratory and bred at the vivarium at the University of Vermont. F1 hybrids were generated by breeding female B6 with male iNOS-KO and female 11.2 with male iNOS-KO. The length and coordinates of the PWD-derived interval on chromosome 11 in 11.2 subconsomic/congenic mice were determined using genotyping at the DartMouse Core Facility (Dartmouth College, Hanover, NH), as previously described (34, 39).

Mice were maintained under specific pathogen–free conditions under protocols approved by Institutional Animal Care and Use Committees. Mice were sacrificed between 6- and 12-wk of age using carbon dioxide and cervical dislocation.

Differentiation and stimulation of murine bone marrow–derived DCs

Murine femurs were sterilized, clipped at one end, and centrifuged at 21,000 × *g* for 15 s to flush bone marrow. Bone marrow was resuspended in complete DC medium (RPMI 1640 containing 10% FBS, 2 mM L-glutamine, 100 Units/ml penicillin, 100 μg/ml streptomycin, and 55 μM 2-ME, all from Life Technologies). DCs were differentiated in 20 ng/ml GM-CSF, either from in-house conditioned media generated by P3X63Ag8.653 cells (catalog no. CRL-1580; American Type Culture Collection [ATCC]) or recombinant cytokine (catalog no. 200-15; Shenandoah Biotechnology). We seeded 1 × 10^7 cells per 10-cm dish (three to five dishes per mouse, depending on the experiment) in an initial volume of 10 ml, added 10 ml on day 2, swapped 15 ml on day 4, and harvested on day 7 by mechanical scraping. For stimulation, seeding density and plate size is indicated in respective methods sections for each assay. The TLR4 ligand LPS from *Escherichia coli* 0111:B4 (LPS) was added at several concentrations that are indicated in the figures (catalog no. tlrl-eblps; InvivoGen). The iNOS inhibitor *S*-ethyl-isothiourea (SEITU) was used at 500 μM (catalog no. 81275; Cayman Chemical). For detection of cytokine accumulation by flow cytometry, the protein transport inhibitor GolgiPlug was used at a dilution of 1:1000 (catalog no. 555029; BD Biosciences).

Human DC culture and activation

Human monocyte-derived DCs (moDCs) were isolated from peripheral blood monocytes by using Miltenyi MACS CD14 positive selection MicroBeads, human, as in (14). Briefly, blood filters from donors were generously donated by Champlain Valley Physicians Hospital Medical Center Blood Bank in Plattsburgh, NY. Filters were reverse-flushed in sterile PBS, and PBMCs were prepared by Ficoll-Paque (density gradient of 1.0772) centrifugal separation using LSM media (MP Biomedicals and Thermo Fisher Scientific). Monocytes were enriched using CD14 positive selection MicroBeads per manufacturer instructions (Miltenyi Biotec) and cultured in complete DC medium supplemented with human GM-CSF (20 ng/μl) plus human IL-4 (20 ng/μl) (Shenandoah Biotechnology) for 7 d. On day 7, moDCs were harvested, stimulated with 100 ng/ml of LPS (L_{100}) for 24 h, and analyzed for nitrite accumulation and extracellular flux analysis (Seahorse) as indicated.

Nitrite quantification

Ninety-six-well plates were seeded with 2 × 10^5 cells per well and stimulated for the indicated duration of time. Media supernatant was harvested and stored at −20°C prior to running the assays. Nitrite content was measured using the Griess nitrite assay according to manufacturer instructions (catalog no. G7921; Molecular Probes).

Quantitative RT-PCR

Twenty-four-well plates were seeded with 1×10^6 cells per well and stimulated for 4 h. CellStripper was used to harvest cells (catalog no. 25058; Corning), which were then centrifuged at 400 × *g* for 5 min to pellet. Pellets were stored at −20°C prior to RNA extraction. RNA was extracted according to the manufacturer's instructions for the QIAGEN RNeasy Mini Kit (catalog no. 74104; QIAGEN) and RNase-Free DNase Set (catalog no. 79254; QIAGEN). Sample concentration was determined by NanoDrop (NanoDrop 2000 Spectrophotometer; Thermo Fisher Scientific), and 200 ng of RNA was used in the cDNA synthesis reaction according to the manufacturer's instructions for the qScript cDNA SuperMix Kit (catalog no. 95047; Quantabio). The quantitative RT-PCR (RT-qPCR) reaction was performed according to the manufacturer's instructions for the DyNAmoColor-Flash SYBR Green (catalog no. F416S; Thermo Fisher Scientific) Kit, using the specified *Nos2* and β-2 microglobulin primers and 1 μl of product from the cDNA synthesis reaction (primers from Thermo Fisher Scientific). The RT-qPCR was run on a QuantStudio 3 Real-Time PCR System (96-well, 0.2 ml; catalog no. A28137; Thermo Fisher Scientific). We calculated the δ Ct between the housekeeping gene *B2m* (β-2 microglobulin) and *Nos2*, then calculated the expression of *Nos2* relative to *B2m* as $2^{-(\delta\ Ct)}$.

Flow cytometry

Ninety-six–well plates were seeded with 2×10^5 cells per well and stimulated for the indicated duration of time. Cells were incubated in CellStripper (catalog no. 25058; Corning) for 20 min prior to transferring to round bottom ninety-six–well plates for staining. Cells were washed with serum-free PBS and resuspended 1:2000 in fixable viability stain in PBS for 30 min (catalog no. L34961; Molecular Probes/Invitrogen). Cells were washed with PBS containing 1% FBS (hereafter called 1% FBS) at 400 × *g* for 5 min and then fixed in PBS containing 1% formaldehyde for 15 min (catalog no. 30525-89-4; Alfa Aesar). For intracellular staining, cells were permeabilized in 0.2% saponin (catalog no. S-7900; Sigma-Aldrich) in PBS for 10 min, and Perm/Wash (catalog no. 51-2091-KZ; BD Biosciences) was used for all wash steps and Ab incubations. For extracellular staining, 1% FBS was used for all wash steps and Ab incubations. Prior to all Ab incubations, cells were incubated for 10 min with TruStain FcX PLUS (anti-mouse CD16/32) Ab (catalog no. 156604; BioLegend) at 1:200 to block Fc receptors. All Ab incubations were 30 min at room temperature as follows: CD11c-PE/Cy7 (1:800; catalog no. 117318; BioLegend), CD11b–allophycocyanin/Cy7 (1:3333; catalog no. 557657; BD Pharmingen and catalog no. 101226; BioLegend), IL-12–allophycocyanin (1:400; catalog no. 505205; BioLegend), and TNF-PE (1:400; catalog no. 506305; BioLegend). MitoTracker Deep Red FM staining was performed according to manufacturer's instructions (catalog no. M222426; Invitrogen). Intracellular iNOS staining involved sequential incubation with anti-iNOS primary (1:2000; catalog no. SC-7271; Santa Cruz Biotechnology) followed by anti-mouse IgG-PE (1:200; catalog no. 406608; BioLegend). Single-color controls were prepared in parallel with samples and underwent all incubation and wash steps. For the viability dye single-color control, cells were heat killed at 55°C for 15 min and then pooled in an equal ratio with live cells prior to staining and fixation. Samples were run on an LSR II (BD Biosciences) or an Aurora (Cytek Biosciences). All flow analysis was performed using FlowJo Software version 10.6.1 (BD Biosciences).

Western blot

Six-well plates were seeded with 2×10^6 cells per well and stimulated for 24 h. Mechanical scraping was used to transfer cells to tubes for centrifugation at 400 × *g* for 5 min. Supernatant was aspirated, and pellets were either frozen at −20°C or immediately resuspended in 100 μl of Cell Lysis Buffer (catalog no. 9803; Cell Signaling Technology) containing Pierce Protease and Phosphatase Inhibitors (catalog no. A32959; Thermo Fisher Scientific). Samples were vortexed and kept on ice for 30 min and then, following a 9600 × *g* spin for 10 min, supernatant was transferred to new tubes. Protein concentration was assayed using a Pierce BCA Assay Kit according to manufacturer's instructions (catalog no. A32959; Thermo Fisher Scientific), and all samples were normalized to 0.5 mg/ml in sample buffer containing 2-ME. Samples were heated at 95°C for 5 min prior to loading a 7.5% MP TGX precast polyacrylamide gel (catalog no. 4561023; Bio-Rad Laboratories) with a 10-μl ladder (catalog no. 161-0375; Bio-Rad Laboratories) or a 30-μl sample per well. Samples ran at 120V for 60 min and were then transferred onto nitrocellulose membranes, according to manufacturer's instructions (catalog no. 1704270; Bio-Rad Laboratories) using a Trans-Blot Turbo Transfer System (catalog no. 1704150; Bio-Rad Laboratories). Five percent BSA in TBST was used for blocking and all Ab incubations. Overnight incubations in primary Abs iNOS (1:1000; catalog no. 2982S; Cell Signaling Technology) and β-actin (1:2000; catalog no. 643802; BioLegend) were followed by washing with TBST and then 1-h incubations in secondary Abs HRP anti-rabbit (1:1000) and HRP anti-mouse (1:5000; catalog no. 405306; BioLegend). SuperSignal West Pico PLUS Chemiluminescent Substrate (catalog no. 34579; Thermo Fisher Scientific) was used for detection, and blots were imaged on a Syngene PXi.

L. monocytogenes

L. monocytogenes strains ATCC 19115 and F5817 were used for all bacterial experiments. Cultures were grown from frozen stocks in brain heart infusion broth (catalog no. R45272; Remel) at 37°C in an orbital shaker. Bacteria were quantified using OD 600 readings. Cultures were washed and resuspended in antibiotic-free media prior to cell incubation. For all experiments, bacteria were incubated with DCs at a multiplicity of infection (MOI) of 1. For in vivo replication studies, a modified gentamicin protection assay was performed. Bacteria and DCs were incubated for 1 h at 37°C to allow bacterial internalization. Cells were washed and then incubated in 50 μg/ml gentamicin for 30 min. Cells were washed again and incubated for 18 h in antibiotic-free media in the presence and absence of the iNOS inhibitor SEITU. Cells were subsequently washed, and DCs were lysed in 200 μl of sterile water. For relative bacterial counts, brain heart infusion agar plates were plated overnight with 20 μl of a 1:100 dilution of lysate, and colonies were counted on the next day.

Extracellular flux analysis

Seahorse plates were seeded with 2×10^5 cells per well and stimulated overnight. The extracellular acidification rate and oxygen consumption rate (OCR) were measured with a metabolic flux analyzer (24XP and/or 96XP; Seahorse Bioscience, North Billerica, MA). Mitochondrial stress tests were performed according to the manufacturer's instructions.

Metabolomics

Cells were differentiated as above and shifted to glucose-free media containing 5 mM $[^{13}C]_6$ glucose at the time of stimulation for the indicated duration. Frozen cell pellets were extracted at 2×10^6 cells/ml in ice-cold lysis/extraction solution (methanol/acetonitrile/water 5:3:2 [v/v/v]). Supernatants were clarified by centrifugation (10 min, 18,000 × *g*, 4°C), and 10 μl was analyzed using a Thermo Fisher Scientific Vanquish ultra-high-performance liquid chromatography (UHPLC) coupled to a Thermo Fisher Scientific Q Exactive mass spectrometer. Global metabolomics analyses were performed using a 5-min C18 gradient in positive and negative ion modes (separate runs) with electrospray ionization as described. For all analyses, the mass spectrometry (MS) scanned in MS1 mode across the m/z range of 65 to 950. Metabolite assignments and isotopologue distributions were annotated in conjunction with the Kyoto Encyclopedia of Genes and Genomes database, integrated, and quality control was performed using Maven (Princeton University) as previously described (40, 41). Relative quantitation was performed by exporting the values for integrated peak areas of light metabolites and their isotopologues into Excel (Microsoft, Redmond, CA), upon correction for natural abundance of ^{13}C, for statistical analysis.

Protein sequence alignments

The Jackson Laboratory's Mouse Phenome Database (genome assembly GRCm38mm10) genotype query tool was used to identify single nucleotide polymorphisms (SNPs) in *Nos2* between B6 and PWK/PhJ (PWK). We chose to use PWK as a surrogate for PWD, as their genomes are highly similar (37), but PWK is much more densely genotyped by sequencing (42). We constrained our query to nonsynonymous mutations to generate a list of polymorphic amino acids and associated single nucleotide polymorphism database (dbSNP) RS identification numbers. The dbSNP RS identification numbers were cross-referenced with both Ensembl and UniProt to determine the correct amino acid positions. Next, we pulled B6 (UniProtKB P29477) and Human (UniProtKB P35228) iNOS sequences from UniProt. To generate a PWK protein sequence we duplicated the B6 sequence and introduced the amino acid changes identified by the Mouse Phenome Database SNP query (see above). We performed multiple sequence alignment on these three FASTA sequences using a program called T-Coffee, which generates the output as a fasta_aln file. We then input the fasta_aln file into a program called Boxshade to highlight the polymorphic amino acids. Table I displays the polymorphic amino acids between these three sequences, and the full alignment is displayed in Supplemental Table I. For comparisons of *Nos2* alleles across inbred mouse strains, The Jackson Laboratory's Mouse Phenome Database (genome assembly GRCm38mm10) was used to identify SNPs in *Nos2* between the following classical (B6, 129S1/SvInJ, A/J, BALB/cJ, NOD/ShiLtJ, and NZO/HILtJ) and inbred (PWK, CAST/EiJ, WSB/EiJ) strains. For Table II, we queried for nonsynonymous mutations in *Nos2*. As unshown data, we also queried *Nos2* plus 10,000 bp flanking either end and did not filter on dbSNP functional annotation.

ELISA

The concentration of TNF in the media supernatant of stimulated DCs was determined by sandwich ELISA using the following reagents: TNF capture Ab (1:250; catalog no. 506102; BioLegend), TNF detection Ab (1:2000; catalog no. 516003; BioLegend), streptavidin (1:40; R&D Systems), peroxidase TMB Substrate and Peroxide Solution (Thermo Fisher Scientific catalog nos.1854050 and no. 1854060, mixed in equal parts).

Quantification and statistical analysis

Throughout, "*n*" refers to independent cell cultures from individual mice, with the exception of a few replicate experiments in which individual femurs from one mouse were cultured and differentiated separately as biological replicates. All statistical tests were performed in GraphPad.

Results

The assumption that the rapid and robust production of NO in activated subsets of DCs is a cardinal feature of the mouse immune response is tenuously predicated on the premise that the B6 strain is an appropriate representative model in this context. In these studies, we question whether this phenotype is an artifact, perhaps resulting from the loss of evolutionary pressure during ~150 y of domesticity and inbreeding in sterile environments. Genetic variation among the human population drives phenotypic variation, and this is something that is inadequately modeled by studies within a single inbred mouse strain. To investigate whether NO-mediated changes in mitochondrial respiration, carbon metabolism, and postactivation survival are a preserved feature across DCs from genetically diverse mouse strains, we selected a wild-derived strain from which DCs were assessed for these parameters. We have previously used the wild-derived PWD strain alongside the B6 mouse to assess the influence of genetic variation in our models of inflammatory and autoimmune diseases (34, 35, 43) and have recapitulated those comparisons in this study for similar purposes.

The PWD mouse and human Nos2/NOS2 *alleles encode highly similar iNOS sequences that are distinct from the B6*

To investigate allelic differences in *Nos2* between B6 and PWD, we mined PWK genotype data as a surrogate for PWD because this strain is highly related to PWD (37) and, unlike PWD, has been densely sequenced (42). We found that the PWK *Nos2* allele encodes six nonsynonymous amino acid substitutions compared with the B6 *Nos2* allele (Table I). Strikingly, five of these six substitutions are identical to the differences between the human iNOS protein and the B6 iNOS protein (Table I, full alignment in Supplemental Table I). In addition, the most commonly used inbred laboratory mouse strains (B6, 129S1/SvImJ, A/J, BALB/cJ, NOD/ShiLtJ, and NZO/HILtJ) carry identical haplotypes at the *Nos2* locus, encoding identical iNOS amino acid sequences, whereas there are significant protein coding changes (compared with B6) in wild-derived mouse strains, including PWK, CAST/EIJ, and WSB/EIJ (Table II; full alignment is not shown, but methods are described). These comparisons across mouse species and between the human genome suggest that much of our understanding of the *Nos2* gene and its protein product in B6 mice may be skewed by limited genetic diversity and/or a lack of selective pressure experienced in common laboratory strains over decades. Of note, the same frequency of allelic divergence between wild-derived and common laboratory strains is not observed for the *Arg1* gene, whose protein product competes with iNOS for arginine as a substrate, suggesting that the high variability in the *Nos2* gene among wild-derived strains in unlikely to be random (data not shown). For these studies, we chose to focus our studies on the PWD mouse (compared with B6), as it has the highest protein sequence homology to the human protein compared with other wild-derived strains (Table I).

Human moDCs do not produce detectable levels of NO upon LPS stimulation

To confirm previous reports that human moDCs do not recapitulate the robust NO production seen in the B6 mouse model, we generated moDCs from three human donors and stimulated them for 24 h with LPS. moDCs produced no detectable NO as assayed by nitrite accumulation (Fig. 1A; Griess assay) and showed no evidence of the NO-dependent postactivation suppression of mitochondrial respiration that has been previously published for B6 DCs (Fig. 1B, 1C) (11, 14).

PWD DCs have attenuated iNOS induction and NO production to LPS compared with B6 DCs

To test whether NO is differentially produced in PWD DCs compared with B6 DCs, we stimulated cells from both genetic backgrounds with LPS and performed a Griess assay to quantify nitrite accumulation in the media from these cultures. Whereas neither genotype exhibited detectable NO levels in the absence of stimulation, PWD DCs produced significantly lower amounts of NO compared with B6 DCs at 48 h post-LPS stimulation (Fig. 1D). To test whether these NO differences are a function of differential transcriptional regulation of the *Nos2* gene between B6 and PWD DCs, we performed RT-qPCR on DCs stimulated for 4 h with LPS and observed significantly lower *Nos2* gene expression in PWD DCs than B6 DCs (Fig. 1E). In accordance with this, the percentage of $iNOS^+$ DCs determined by flow cytometry was significantly lower in PWD DCs than B6 DCs (Fig. 1F). Taken together, these results suggest that low NO production in PWD DCs is the result of reduced *Nos2* mRNA and iNOS protein levels compared with B6 DCs.

We have previously published that NO production in B6 DCs causes inhibition of mitochondrial respiration and increased use of glycolysis for sustained postactivation survival (11, 14). Furthermore, we have postulated that there exists a mitochondrial inhibitory

Table I. The PWK *Nos2* gene contains six amino acid substitutions compared with the B6, five of which are present in the human *NOS2* sequence

dbSNP RS number	Amino Acid Position	C57BL/6J	PWK/PhJ	Human
rs222693626	72	-	P	P+L
rs263111341	136	H	Q	Q
rs28228005	652	E	K	E
rs247031120	692	F	Y	Y
rs239776991	884	H	R	R
rs240568889	1060	N	S	S
rs28227949	1075	I	V	V

Nonconservative SNPs in B6, PWK, and human *Nos2/NOS2* sequences identified using The Jackson Laboratory's Mouse Phenome Database. See *Materials and Methods* for more information. See Supplemental Table I for full protein sequence alignment.

Table II. Nonconservative amino acid substitutions in *Nos2* between the following classical (B6, 129S1/SvInJ, A/J, BALB/cJ, NOD/ShiLtJ, and NZO/HILtJ) and inbred (PWK, CAST/EiJ, and WSB/EiJ) strains

				Common Inbred Strains						Wild Derived Strains		
Chromosome location	dbSNP RS		Amino Acid Position	C57BL/6J	129S1/SvInJ	A/J	BALB/cJ	NOD/ShiLtJ	NZO/HILtJ	PWK/PhJ	CAST/EiJ	WSB/EiJ
11:78931687	rs263111341	A/T	136	T	T	T	T	T	T	A	A	T
11:78939979	rs262549152	G/T		G	G	G	G	G	G	G	T	T
11:78948325	rs28228005	A/G	652	G	G	G	G	G	G	A	G	G
11:78949141	rs247031120	A/T	692	T	T	T	T	T	T	A	A	T
11:78949183	rs240287546	C/T		T	T	T	T	T	T	T	C	T
11:78951218	rs28227983	C/T		C	C	C	C	C	C	C	C	T
11:78952879	rs239776991	A/G	884	A	A	A	A	A	A	G	G	A
11:78952989	rs28227976	A/G		G	G	G	G	G	G	G	A	G
11:78955389	rs28227960	A/G		A	A	A	A	A	A	A	G	G
11:78957447	rs240568889	A/G	1060	A	A	A	A	A	A	G	A	A
11:78957491	rs28227949	A/G	1075	A	A	A	A	A	A	G	G	G

Nonconservative SNPs identified using The Jackson Laboratory's Mouse Phenome Database. See *Materials and Methods* section for more information.

threshold for NO production, above which mitochondrial respiration is fully impaired and below which mitochondrial function is maintained (15). We hypothesized that the low NO levels produced by PWD DCs would allow for retention of mitochondrial respiration. To assess whether there are intrinsic mitochondrial respiration differences between the strains, we measured the basal OCR of unstimulated DCs and found that PWD DCs exhibit significantly elevated basal respiration rates compared with B6 DCs (Fig. 1G). To explicitly compare mitochondrial function in DCs from both strains, we performed a mitochondrial stress test using extracellular flux analysis as previously published (15). In unstimulated DCs from both strains, comparable functional mitochondrial responses were observed (Fig. 1H, left). However, whereas LPS-stimulated B6 DCs exhibited a complete loss of mitochondrial respiration (Fig. 1H, center), iNOS inhibition partially restored mitochondrial respiration in LPS-stimulated B6 DCs, which is consistent with previous reports (Fig. 1H, right) (11, 15). Consistent with their low NO production, LPS-stimulated PWD DCs completely preserved their mitochondrial respiration (Fig. 1H, 1I).

The congenic 11.2 strain recapitulates the NO phenotype of PWD DCs

Assessment of lineage markers CD11c and CD11b confirmed that B6 and PWD DCs are composed of subtle but reproducibly different phenotypic population frequencies (Supplemental Fig. 1B, 1C). Specifically, PWD DC cultures yield more $CD11b^{+}CD11c^{-}$ subsets than are found in conventional B6 cultures. These differences are relatively unsurprising, considering the substantial genetic polymorphism between B6 and PWD; the SNP rate between these strains is 0.92 per 100 bp (44) and thus makes a direct comparison of B6 and PWD DCs challenging. Our laboratory has previous experience using congenic and consomic strains that carry single or partial PWD chromosomes on the B6 genetic background (45). This tool enables the analysis of genetic polymorphisms driving phenotypes of interest while eliminating additional genetic variation, thereby allowing for the focused study of a single genetic region. To test whether PWD alleles at the *Nos2* locus were sufficient to drive differential NO production in PWD DCs, we selected the congenic 11.2 strain, which carries a PWD-derived interval spanning from 43.8 to 99.7 Mb on chromosome 11 (including $Nos2^{PWD}$ at 78.81–78.85 Mb) on an otherwise B6 genetic background (Supplemental Fig. 1A). We confirmed that unstimulated B6 and 11.2 DCs had comparable expression of lineage markers CD11c and CD11b (Supplemental Fig. 1B, 1C).

To test whether potential differences in iNOS induction between B6 and 11.2 DCs are explained by differential TLR responsiveness to LPS, we measured nitrite production and postactivation mitochondrial respiration over a range of LPS concentrations (Fig. 2A, 2B). Nitrite production was notably distinct between the two strains at 10 ng/ml LPS (L_{10}) but less so at higher concentrations, and this was concomitant with preserved mitochondrial respiration in 11.2 DCs at this dose but not in B6 DCs (Fig. 2B). Importantly, DCs from both strains exhibited lost mitochondrial respiration at higher doses of LPS (Fig. 2B). From these findings, we chose to use both a lower dose of LPS (L_{10}) and a higher dose of LPS (L_{100}) to explore these differential states of NO production and NO-dependent cell respiration for our studies. We saw comparable proinflammatory cytokine expression in B6, 11.2, and PWD DCs stimulated with L_{10} and L_{100}, suggesting that TLR activation of PWD DCs is intact and that differential NO production is not a function of global differences in LPS responsiveness and activation states (Supplemental Fig. 2).

11.2 DCs exhibit attenuated NO production

In both B6 and 11.2 DCs, nitrite levels increased in an LPS dose-dependent manner, indicating that NO production is proportionally regulated by the level of inflammatory stimulus encountered (Fig. 2C). At L_{10} and L_{100}, nitrite levels from 11.2 DCs were significantly lower than from B6 DCs; thus, 11.2 DCs partially recapitulate the restrictive iNOS regulation seen in PWD DCs (Fig. 2C). At L_{10}, 11.2 DCs appear to make very little NO as measured by nitrite accumulation, whereas they show around 35% reduction in nitrite accumulation at L_{100} compared with B6 controls (Fig. 2C). Because NO is a highly diffusible molecule that can react with many potential cellular targets, the Griess nitrite assay, which serves as one indicator of NO production, does not necessarily capture or reflect the totality of NO production in this cellular system. Recent work in activated macrophages demonstrated that citrulline, which is the direct byproduct of arginine metabolism during NO generation by iNOS, is a reliable indicator of NO production (46, 47). We employed UHPLC-MS to measure citrulline abundance following stimulation in the presence or absence of an iNOS inhibitor SEITU. Our results showed that the measurable citrulline levels detected in LPS-stimulated DCs are exclusively the result of iNOS activity, as iNOS inhibition completely eliminates measurable intracellular citrulline (Fig. 2D). In agreement with the Griess assay, we measured lower citrulline levels by UHPLC-MS in 11.2 DCs than B6 DCs (Fig. 2D); however, appreciable citrulline levels were detected at L_{10} in 11.2 DCs, which suggests the following: 1) the UHPLC-

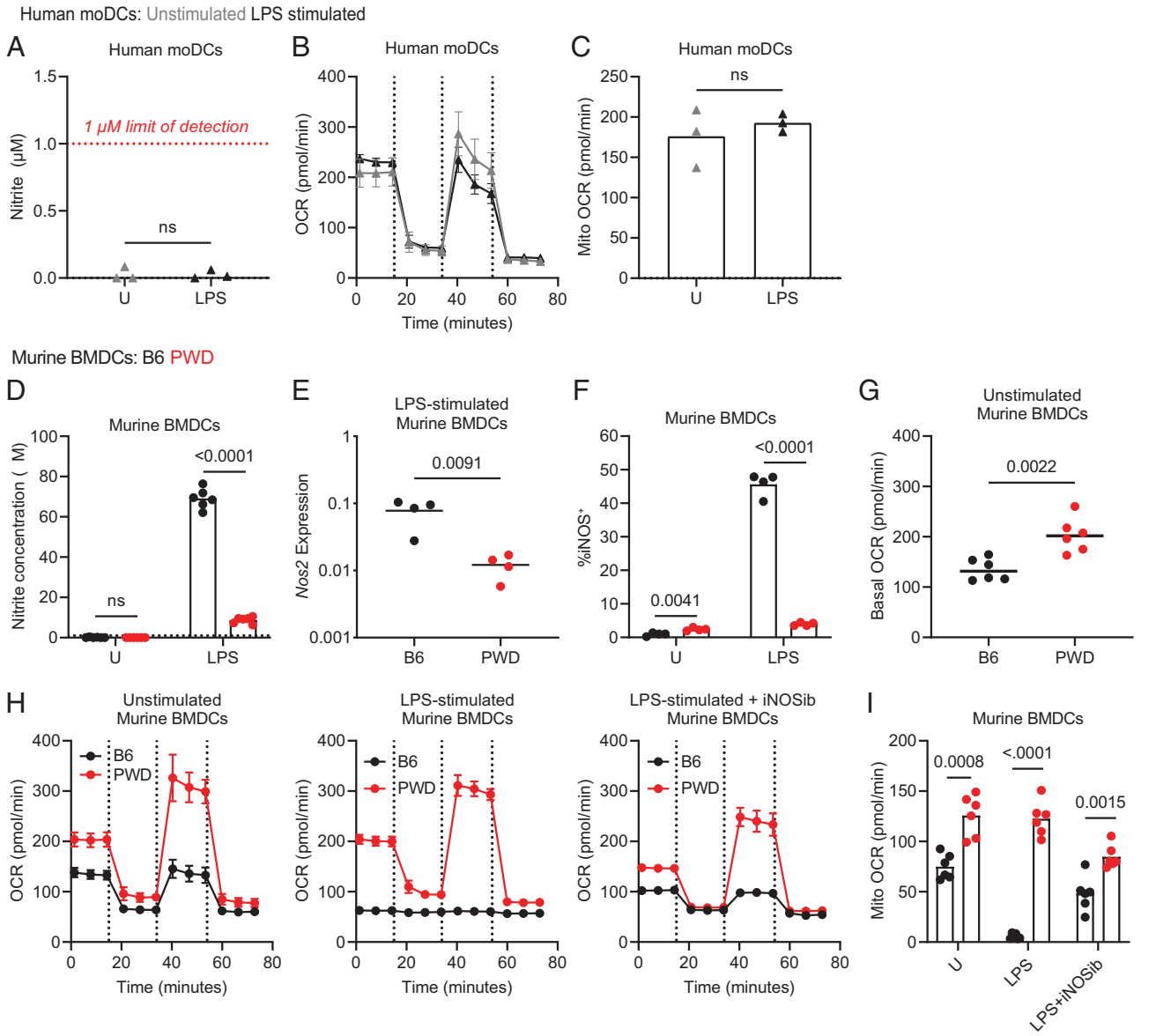

FIGURE 1. iNOS induction and NO production in LPS-stimulated human DCs and PWD mouse DCs is attenuated compared with B6 DCs. (**A**) Griess nitrite assay on media supernatant from human moDCs from three human donors stimulated for 24 h with U and L_{100}. Horizontal dotted line indicates 1-μM limit of detection. Analyzed by *t* test, *p* value is reported (*p* value > 0.05 is ns). $n = 3$. Color key above (A) applies to (A)–(**C**). (B) Mitochondrial stress test kinetic trace of extracellular flux analysis on human moDCs in (A). Injections are indicated by dashed vertical lines. $n = 3$. (C) Mitochondrial-dependent OCR calculated from the kinetic trace in (B) by subtracting OCR postinhibition of the electron transport chain from resting OCR prior to injections of mitochondrial inhibitors. Analyzed by *t* test, *p* value is reported (*p* value > 0.05 is ns). $n = 3$. (**D**) Griess nitrite assay on media supernatant from DCs stimulated for 48 h with U and L_{100}. Horizontal dotted line indicates 1-μM limit of detection. Analyzed by multiple *t* tests, adjusted *p* values are reported (*p* value > 0.05 is ns). $n = 6$, representative of three independent experiments. Color key above (D) applies to (D)–(**I**). (E) *Nos2* gene expression assessed by RT-qPCR on DCs stimulated for 4 h with U and L_{100}. Normalization is $2^{-(\delta\ Ct)}$ with *β-2-microglobulin* used as housekeeping gene. Analyzed by *t* test, *p* value is reported (*p* value > 0.05 is ns). $n = 4$. (F) Flow cytometry was used to identify the percentage of iNOS plus DCs stimulated for 24 h with U and L_{100}. iNOS gate is on $CD11c^{+}CD11b^{+}$ cells. Analyzed by multiple *t* tests, adjusted *p* values are reported (*p* value > 0.05 is ns). $n = 6$, representative of three independent experiments. (G) Extracellular flux analysis was used to assess basal OCR of unstimulated DCs. $n = 6$, representative of three independent experiments. (H) Mitochondrial stress test kinetic traces of extracellular flux analysis on DCs stimulated for 24 h with U, L_{100}, and iNOSib plus L_{100}. Injections are indicated by dashed vertical lines. $n = 6$, representative of three independent experiments. (I) Mitochondrial-dependent OCR calculated from the kinetic traces in (H) by subtracting OCR postinhibition of the electron transport chain from resting OCR prior to injections of mitochondrial inhibitors. Analyzed by multiple *t* tests, adjusted *p* values are reported (*p* value > 0.05 ns). $n = 6$, representative of three independent experiments. basal OCR, unstimulated OCR; iNOSib, iNOS inhibitor SEITU; Mito OCR, mitochondrial-dependent OCR; U, unstimulated.

MS approach is significantly more sensitive at evaluating iNOS biochemical activity than the Griess assay, and 2) 11.2 DCs are active NO producers at L_{10}, despite the minimal levels of detectable nitrite accumulation in the media (Fig. 2C). Together, these data indicate that, using the L_{10} versus L_{100} paradigm employed in these studies, we have established a cellular system in which we can toggle between low and high NO production and investigate the cellular and metabolic consequences of these two different cellular states.

To test whether differential transcriptional regulation of *Nos2* drives differences in NO production between B6 and 11.2 DCs, we performed RT-qPCR and observed similar *Nos2* gene expression in 11.2 DCs and B6 DCs at both L_{10} and L_{100} (Fig. 2E). To

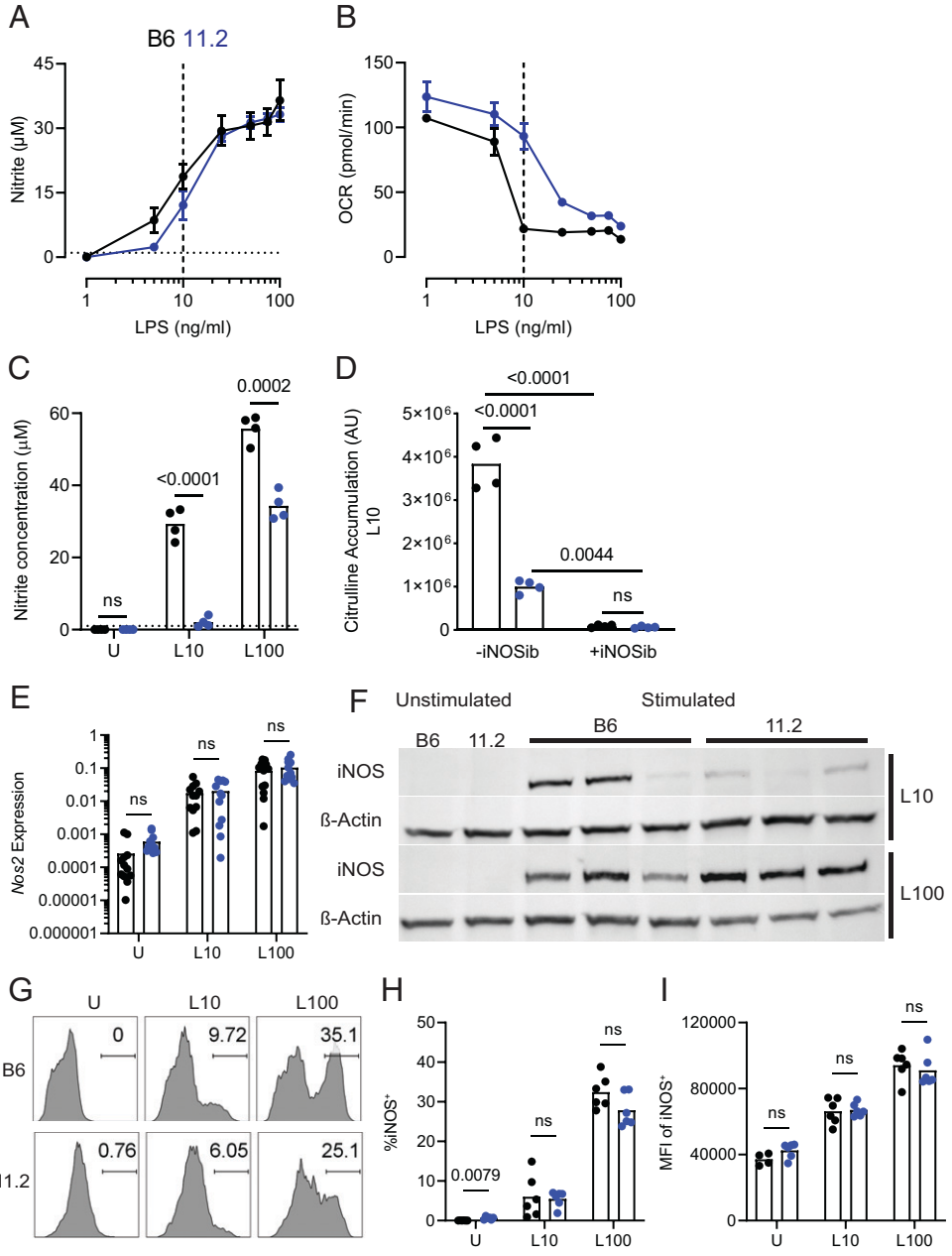

FIGURE 2. NO production in LPS-stimulated 11.2 DCs is attenuated compared with B6 DCs. (**A**) Griess nitrite assay on media supernatant from DCs stimulated for 24 h with a range of LPS doses from 1–100 ng/ml. Horizontal dotted line indicates 1-μM limit of detection. Dashed vertical line indicates L_{10} dose. $n = 6$, representative of two independent experiments. Color key above (A) applies to entire figure. (**B**) Mito OCR calculated from the mitochondrial stress test performed on mouse DCs described in (A). Dashed vertical line indicates L_{10} dose. $n = 6$, representative of two independent experiments. (**C**) Griess nitrite assay on media supernatant from DCs stimulated for 48 h with U, L_{10}, and L_{100}. Horizontal dotted line indicates 1-μM limit of detection. Representative of three independent experiments of $n = 4$. Analyzed by multiple *t* tests, adjusted *p* values are reported (*p* value > 0.05 ns). $n = 4$, representative of two independent experiments. (**D**) Intracellular citrulline levels measured by UHPLC-MS in DCs stimulated for 24 h with L_{10} in the presence or absence of iNOSib. Analyzed by one-way ANOVA and Tukey test, adjusted *p* values are reported (*p* value > 0.05 ns). $n = 4$, representative of one experiment. (**E**) *Nos2* gene expression assessed by RT-qPCR on DCs stimulated for 4 h with U, L_{10}, and L_{100}. Normalization is $2^{-(\delta\ Ct)}$ with *β-2-microglobulin* used as housekeeping gene. Analyzed by multiple *t* tests, adjusted *p* values are reported (*p* value > 0.05 ns). $n = 12$, pooled data from three independent experiments. (**F**) Western blot for iNOS expression in lysates of DCs stimulated for 24 h with L_{10} and L_{100}. β-Actin serves as loading control. $n = 4$, representative of three independent experiments. (**G**) Histogram displays iNOS signal within $CD11c^+CD11b^+$ population of B6 and 11.2 DCs stimulated for 24 h with U, L_{10}, and L_{100}. Gate represents $iNOS^+$ cells. One representative mouse is shown from each strain. (**H**) Quantification of $iNOS^+$ DCs from $CD11c^+CD11b^+$ population shown in (G). Analyzed by multiple *t* tests, adjusted *p* values are reported (*p* value > 0.05 ns). $n = 6$, representative of three independent experiments. (**I**) Quantification of MFI of iNOS signal within the $iNOS^+$ population shown in (H). Analyzed by multiple *t* tests, adjusted *p* values are reported (*p* value > 0.05 ns). $n = 6$, representative of three independent experiments. 11.2, B6.PWD-Chr11.2; AU, arbitrary units; iNOSib, iNOS inhibitor SEITU; MFI, median fluorescent intensity; U, unstimulated.

complement these gene expression studies, we evaluated iNOS protein expression by flow cytometry and Western blot analysis. The Western blot revealed reduced iNOS expression in 11.2 DCs at L_{10} compared with B6 DCs but comparable or even higher protein expression at L_{100} than B6 DCs (Fig. 2F). Intracellular flow cytometry revealed that B6 and 11.2 DCs have no significant difference in the percentage of $iNOS^+$ cells at both L_{10} and L_{100} (Fig. 2G, 2H). The discrepancy between the Western blot and flow cytometry data

are notable but as yet unexplained in our system (Fig. 2F–I). We assessed iNOS expression on a per cell basis by measuring the median fluorescence intensity of $iNOS^+$ cells. We found similar iNOS levels at L_{10} and L_{100} in DCs from both strains (Fig. 2I). Taken together, these results suggest that the differences in NO production between activated B6 and 11.2 DCs are likely driven by posttranscriptional mechanisms.

Restrained NO production in 11.2 DCs results in preserved mitochondrial respiration and enhanced postactivation survival

We have previously published that there appears to be a threshold of NO production above which cells lose virtually all mitochondrial respiration and below which mitochondrial respiratory function is preserved (15). Furthermore, preservation of mitochondrial function correlates with enhanced metabolic flexibility and enhanced postactivation survival in DCs (15). To test whether restrained NO production in 11.2 DCs would result in preserved mitochondrial function, we performed extracellular metabolic flux analysis using a conventional mitochondrial stress test on B6 and 11.2 DCs, either left unstimulated or stimulated at L_{10} or L_{100} (Fig. 3A). Unstimulated DCs exhibited strong functional respiration that was comparable between strains (Fig. 3A, left). At L_{10}, B6 DCs had dramatically impaired respiration, whereas 11.2 DCs had similar respiration to unstimulated cells (Fig. 3A, center). At L_{100}, DCs from both strains had fully blocked mitochondrial respiration (Fig. 3A, right). At both doses of LPS, stimulation in the presence of iNOS inhibitor was able to prevent NO-mediated loss of mitochondrial respiration in DCs from both strains (Fig. 3B). These observations are quantified by the measurement mitochondrial-dependent OCR (Fig. 3C), which is calculated as the difference between the resting OCR and the OCR levels following the addition of electron transport chain inhibitors rotenone (complex I inhibitor) and antimycin A (complex III inhibitor) (Fig. 3C).

To test whether mitochondrial respiratory differences may be related to intrinsic respiratory differences between the strains prior to activation, we measured the basal OCR of unstimulated DCs from both strains and found that 11.2 DCs do exhibit slight but significantly higher basal respiration rates (Fig. 3D). To assess whether the respiratory differences could be a function of differential mitochondrial content between the strains, we measured mitochondrial mass with MitoTracker dye by flow cytometry and saw that signal intensity was not significantly different between strains prior to stimulation (Fig. 3E). The lack of increased mitochondrial mass in 11.2 DCs suggests that this is not a mechanism of preserved respiration in these cells.

Previous studies by our group and others have shown that survival of activated DCs is impaired by iNOS activity and is enhanced by iNOS inhibition (11, 15). We thus hypothesized that activated 11.2 DCs would have higher survival rates than B6 DCs. We used flow cytometry to assess day 4 viability and saw no difference in survival between unstimulated B6 DCs and 11.2 DCs (Fig. 3F, left). In accordance with the mitochondrial respiratory state (Fig. 3A), B6 DCs were nearly all dead 4 d postactivation at L_{10}, whereas there was no significant NO-mediated death in 11.2 DCs at this dose (Fig. 3F, center). In contrast, both genotypes succumbed to iNOS-dependent cell death at L_{100} (Fig. 3F, right). Inhibition of iNOS activity rescued survival of B6 DCs at L_{10} and L_{100} as well as 11.2 DCs at L_{100} (Fig. 3F), confirming the iNOS dependence of this phenotype. Taken together, these results suggest that allelic differences between 11.2 and B6 strains can drive dramatically different iNOS-dependent metabolic reprogramming of mitochondrial activity in DCs, ultimately resulting in their differential survival.

Allelic differences intrinsic to the PWD Nos2 locus contribute to attenuated NO production in 11.2 DCs

The 11.2 congenic PWD-derived interval spans 55.9 Mb and contains 967 protein-coding genes that have the potential to regulate iNOS induction or activity. To address this possibility, we performed heterozygote genetic complementation experiments in which we generated F1 offspring from B6 iNOS-deficient mice (iNOS-KO) crossed with B6 (B6.iNOS-KO.F1, referred to as F1-B6), as well as iNOS-KO crossed with 11.2 (11.2.iNOS-KO.F1, referred to as F1-11.2) pairings (depicted in Supplemental Fig. 3A). We hypothesized that if differential iNOS activity was regulated by regions of the 11.2 PWD interval outside of the *Nos2* locus, then the F1-B6 and F1-11.2 DCs would exhibit comparable NO production because of heterozygous complementation by the B6 portion of the 11.2 segment from the iNOS knockout F1 parent. We observed lower NO production in F1s than the parental strains (Supplemental Fig. 3B), presumably due to only a single functional *Nos2* allele. Therefore, we proceeded to use L_{100} (rather than L_{10}) for these studies. We assessed nitrite accumulation from L_{100}-stimulated B6, 11.2, F1-B6, and F1-11.2 DCs (Supplemental Fig. 3B). F1-B6 DCs, which carry only one functional iNOS allele, had reduced nitrite accumulation compared with B6 DCs and produced nitrite at a level comparable to homozygous 11.2 DCs (Supplemental Fig. 3B). However, the accumulation of nitrite trended lower in F1-11.2 DCs compared with F1-B6 DCs (Supplemental Fig. 3B), demonstrating that complementation by *Nos2*-flanking PWD genes with B6 genes (from iNOS-KO) does not rescue lower NO production by the $Nos2^{PWD}$ allele. In addition, the previously established lack of sensitivity of the Griess assay (Fig. 2C, 2D) may be a limitation of the precise ability to discriminate subtle but meaningful NO production differences.

We next tested whether differential NO production between F1-B6 and F1-11.2 DCs differentially impacts mitochondrial function in these cells. Prior to stimulation, we assessed basal OCR of DCs from both strains to evaluate baseline mitochondrial respiration and did not see differences between F1-B6 and F1-11.2 DCs (Supplemental Fig. 3C). Next, we stimulated F1 DCs and measured mitochondrial-linked OCR, which was significantly higher in F1-11.2 DCs than F1-B6 DCs (Supplemental Fig. 3D). We next tested whether there are transcriptional differences between F1-B6 and F1-11.2 DCs that might explain differential NO production. We assessed relative *Nos2* levels in both F1s and saw no difference in transcript levels (Supplemental Fig. 3E). In accordance with our observation of comparable iNOS protein levels between B6 and 11.2 DCs at L_{100} (Fig. 2F–I), we determined that the percentage of $iNOS^+$ cells was comparable between F1-B6 and F1-11.2 DCs (Supplemental Fig. 3F) as was total iNOS protein expression as assessed by Western blot (Supplemental Fig. 3G). Taken together, these findings indicate that differences intrinsic to the *Nos2* locus contribute to low NO production and preserved mitochondrial function in 11.2 and PWD DCs compared with B6 DCs. They further demonstrate that differential NO production by the *Nos2* PWD allele cannot be accounted for by differences in *Nos2*/iNOS expression alone, suggesting that additional posttranscriptional and posttranslational levels of regulation exist (see *Discussion*).

NO production alters TCA cycle flux, even in the context of preserved mitochondrial respiration

Having established a model of differential NO production that does and does not impair mitochondrial respiration, we next assessed how TCA cycle flux is impacted by different states of NO production when flux to the electron transport chain is intact. Activated macrophages experience TCA cycle reprogramming that is mediated by the presence of NO (46, 48, 49). In activated DCs, LPS stimulation initially increases flux of glucose carbons to citrate, but this flux is halted later during activation (10), and it is unclear what processes govern

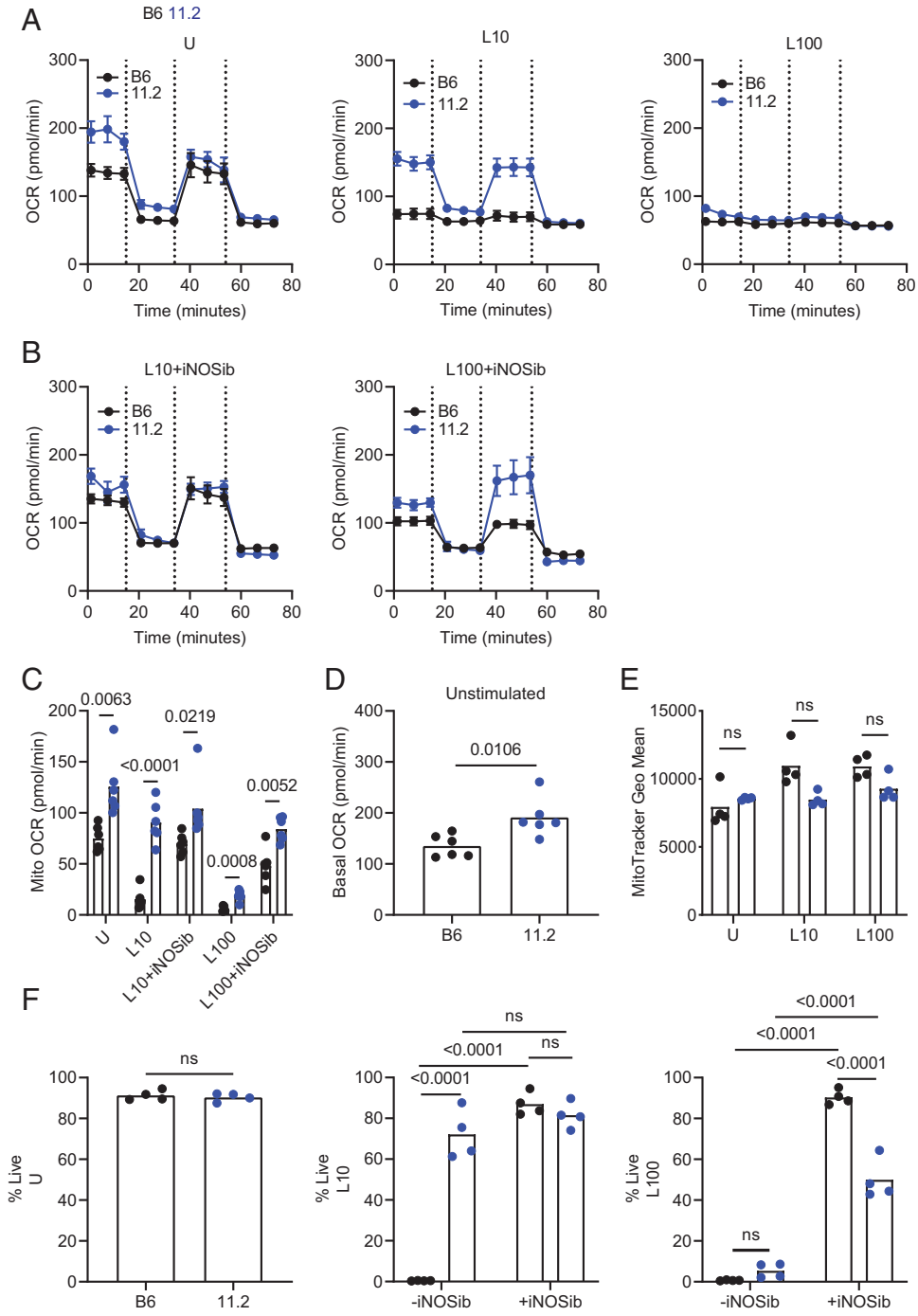

FIGURE 3. Restrained NO production in 11.2 DCs results in preserved mitochondrial respiration and enhanced postactivation survival. (**A**) Mitochondrial stress test kinetic traces of extracellular flux analysis on DCs stimulated for 24 h with U, L_{10}, and L_{100}. Injections are indicated by dashed vertical lines. $n = 6$, representative of three independent experiments. Color key above (A) applies to entire figure. (**B**) Mitochondrial stress test kinetic traces of extracellular flux analysis on DCs stimulated for 24 h with L_{10} plus iNOSib and L_{100} plus iNOSib. Injections are indicated by dashed vertical lines. $n = 6$, representative of three independent experiments. (**C**) Mito OCR calculated from the kinetic traces in (A) and (B) by subtracting OCR postinhibition of the electron transport chain from resting OCR prior to injections of mitochondrial inhibitors. Analyzed by multiple *t* tests, adjusted *p* values are reported (*p* value > 0.05 ns). $n = 6$, representative of three independent experiments. (**D**) Basal OCR of unstimulated DCs assessed by extracellular flux analysis. Analyzed by *t* test, *p* value is reported (*p* value > 0.05 ns). $n = 6$, representative of three independent experiments. (**E**) Flow cytometry was used to assess mitochondrial mass of unstimulated $CD11c^+$ DCs stained with MitoTracker. Analyzed by multiple *t* tests, adjusted *p* values are reported (*p* value > 0.05 ns). $n = 4$. (**F**) Flow cytometry was used to assess survival of DCs stimulated for 96 h by staining with fixable Live/Dead stain. U analyzed by *t* test, *p* value is reported (*p* value > 0.05 ns). L_{10} and L_{100} were analyzed by one-way ANOVA and Tukey test; adjusted *p* values are reported (*p* value > 0.05 ns). $n = 4$, representative of three independent experiments. 11.2, B6.PWD-Chr11.2; basal OCR, unstimulated OCR; geo mean, geometric mean; iNOSib, iNOS inhibitor SEITU; mito OCR, mitochondrial-dependent OCR; U, unstimulated.

citrate accumulation and whether NO plays a role. To test the flux of glucose-derived carbons in different NO-producing cellular states, we used U-[^{13}C]$_6$ glucose tracing to measure the accumulation of labeled carbon atoms in TCA cycle metabolites in B6 and 11.2 DCs stimulated for 24 h at L_{10} in the presence and absence of the iNOS inhibitor SEITU. Nitrite accumulation and citrulline production, two indirect measurements of NO production, are significantly lower in 11.2 DCs than B6 DCs at L_{10} (Fig. 2C, 2D), and as a result, 11.2 DCs

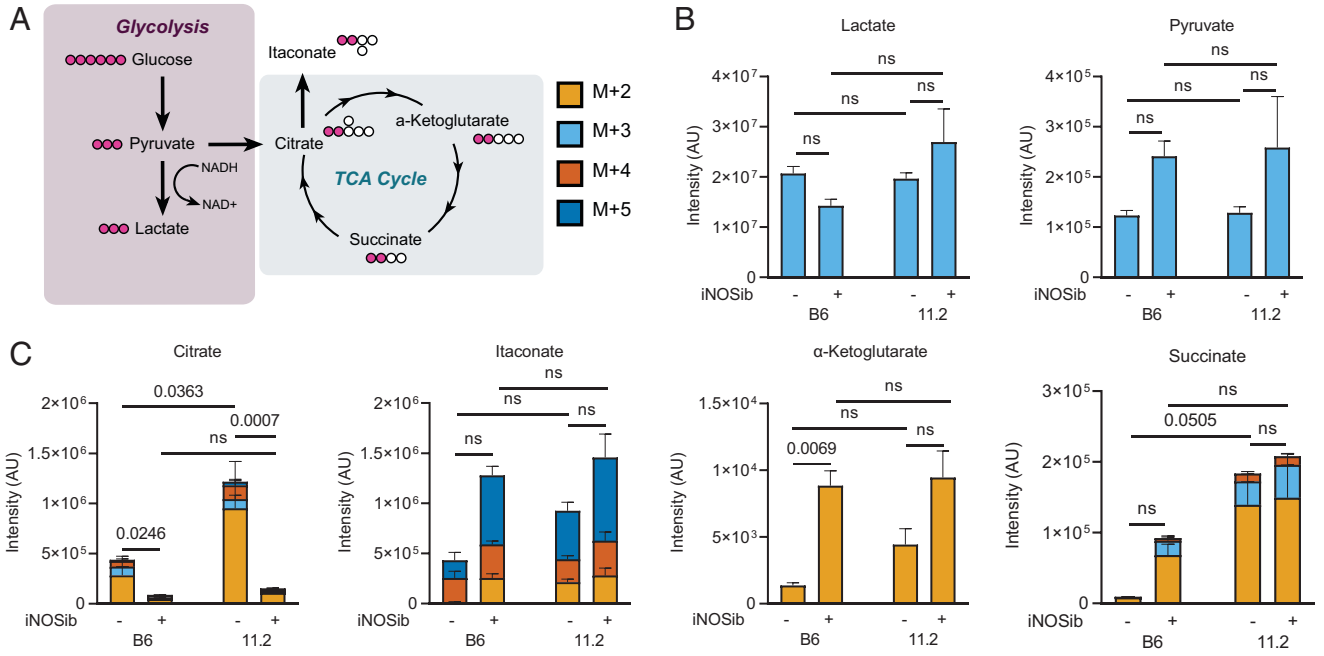

FIGURE 4. NO production alters TCA cycle flux, even in the context of preserved mitochondrial respiration. (**A**) Illustration depicting U[^{13}C]$_6$ glucose tracing experiment. Color key in (A) applies to entire figure. (**B** and **C**) DCs were stimulated for 24 h with L_{10} and L_{10} plus iNOSib in media containing U[^{13}C]$_6$ glucose. UHPLC-MS was used to assess accumulation of heavy carbons in glycolysis and TCA cycle metabolites. Analyzed by one-way ANOVA and Tukey test, adjusted p values are reported (p value > 0.05 ns). $n = 4$, representative of two independent experiments. +2/3/4/5, mass of 2/3/4/5 heavy carbons; 11.2: B6.PWD-Chr11.2; AU, arbitrary units; iNOSib: iNOS inhibitor SEITU; M, metabolite mass.

stimulated at L_{10} maintain mitochondrial respiration, whereas B6 DCs experience complete inhibition of mitochondrial respiration (Fig. 3A). In this U[^{13}C]$_6$ glucose tracing experiment, 11.2 DCs stimulated at L_{10} without the iNOS inhibitor provide the opportunity to study TCA cycle flux (Fig. 4A), comparing intact mitochondrial respiration correlated with low NO production (11.2 DCs) to blocked mitochondrial respiration and high NO production (B6 DCs). We observed that ^{13}C enrichment of glycolysis end- and by-products pyruvate and lactate was comparable between strains, suggesting that these metabolites are not sensitive to NO production differences between B6 and 11.2 cells (Fig. 4B). In contrast, we identified heavy citrate (decreasing), itaconate, α-ketoglutarate, and succinate (increasing) as metabolites that were impacted by NO inhibition (Fig. 4C). Interestingly, glucose-dependent citrate accumulation occurred in DCs from both strains in an NO-dependent manner (Fig. 4C). In addition, we identified citrate, itaconate, α-ketoglutarate, and succinate as metabolites that were impacted (accumulation either increased or decreased) by genotype (11.2 versus B6) and iNOS inhibition (Fig. 4C). Accumulation of the "late" TCA intermediate succinate was higher in 11.2 DCs compared with B6 DCs, and iNOS inhibition partially restored B6 DCs to 11.2-like levels. A similar pattern was observed for glucose-derived itaconate and the TCA intermediate α-ketoglutarate (Fig. 4C). Surprisingly, citrate accumulation was higher in 11.2 DCs compared B6 DCs and was completely relieved by iNOS inhibition in both strains (Fig. 4C). These data uncover the novel observation that low levels of NO production can impact citrate accumulation in a manner that is uncoupled from complete respiratory blockade. Further, the model that an NO respiratory "threshold" impacts postcitrate TCA cycle carbon flux is supported by the increased abundance of [^{13}C]α-ketoglutarate and succinate in 11.2 DCs compared with B6 cells. Additionally, data suggest an impact of genetic divergence between 11.2 and B6 at the levels of reactions controlled by oxoglutarate dehydrogenase and succinate dehydrogenase/complex II with glucose-derived–labeled succinate accumulation being significantly higher in 11.2 mice in presence or absence of iNOS inhibitors.

11.2 DCs exhibit impaired NO-mediated control of pathogen L. monocytogenes

One of the interesting dynamics of the model for differential NO production we have described is the ability to study the tradeoff between NO-mediated mitochondrial toxicity versus NO-dependent antimicrobial function. To consider this tradeoff, we assessed the activation of B6 and 11.2 DCs in a bacterial infection system (Fig. 5). Published studies have established that NO production by activated DCs is critical for the control of *L. monocytogenes* infection (26, 27). Having established that 11.2 DCs make less NO upon LPS activation than B6 DCs, we hypothesized that low NO production in 11.2 DCs would result in less potent NO-mediated bacterial control than B6 DCs. We first tested whether the deficit in nitrite accumulation observed in 11.2 DCs in response to LPS is recapitulated when DCs are activated by infection with *L. monocytogenes*; 11.2 DCs showed a trend toward less nitrite accumulation in response to stimulation with two different strains of *L. monocytogenes* compared with B6 DCs, but this was not statistically significant (Fig. 5A, 5B). To test the prediction that *L. monocytogenes*–stimulated 11.2 DCs maintain mitochondrial respiration, we performed metabolic extracellular flux analysis as above, which demonstrated that 11.2 DCs maintain higher functional respiration than B6 DCs in response to *L. monocytogenes* bacterial stimulation (Fig. 5C, 5D). To test the NO dependence for *L. monocytogenes* replication control in our in vitro DC cultures, we coincubated B6 and 11.2 DCs with two different strains of *L. monocytogenes* for 18 h in the presence or absence of the iNOS inhibitor SEITU and measured relative bacterial counts as an indicator of intracellular bacterial replication/survival. B6 DCs potently restricted *L. monocytogenes* replication/survival during this assay, and this killing capacity was substantially impaired by iNOS inhibition (Fig. 5E, 5F), thus confirming that NO production controls *L. monocytogenes* replication in this model. From these data, we then predicted that 11.2 DCs, by virtue of their restrained NO production, would exhibit impaired control of *L. monocytogenes* replication compared with B6 cells. Bacteria counts

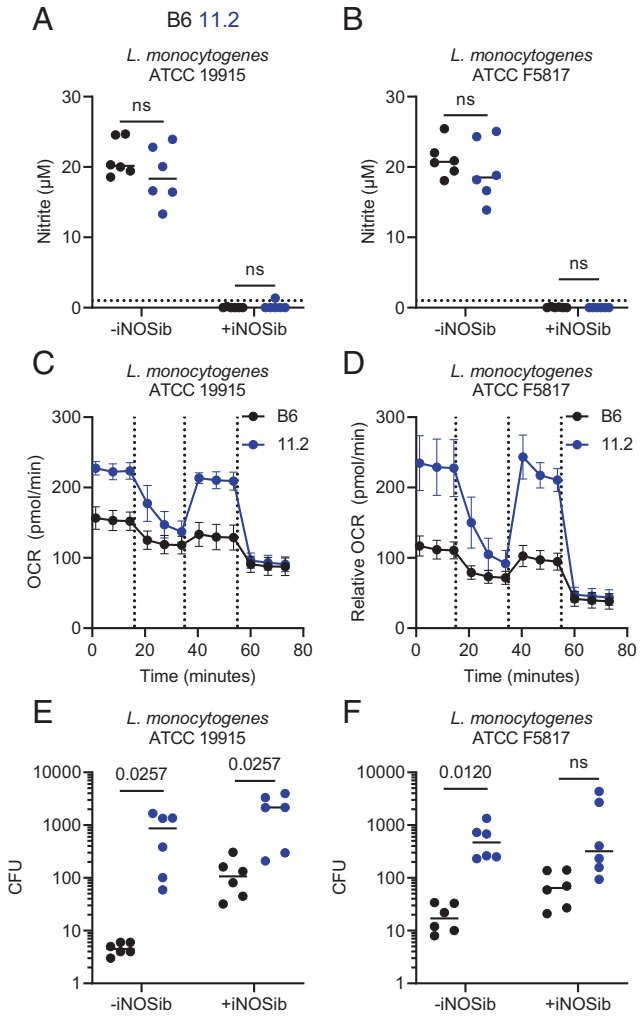

FIGURE 5. 11.2 DCs exhibit impaired NO-mediated control of pathogen *L. monocytogenes*. (**A**) Griess nitrite assay on media supernatant from DCs stimulated for 18 h with *L. monocytogenes* ATCC 19115 at MOI = 1. Horizontal dotted line indicates 1-μM limit of detection. Analyzed by multiple *t* tests, adjusted *p* values are reported (*p* value > 0.05 ns). $n = 6$, representative of two independent experiments. Color key above (A) applies to entire figure. (**B**) Griess nitrite assay on media supernatant from DCs stimulated for 18 h with *L. monocytogenes* ATCC F5817 at MOI = 1. Horizontal dotted line indicates 1-μM limit of detection. Analyzed by multiple *t* tests, adjusted *p* values are reported (*p* value > 0.05 ns). $n = 6$, representative of two independent experiments. (**C**) Mitochondrial stress test kinetic traces of extracellular flux analysis on DCs stimulated for 18 h with *L. monocytogenes* ATCC 19115 at MOI = 1. Injections are indicated by dashed vertical lines. $n = 3$. (**D**) Mitochondrial stress test kinetic traces of extracellular flux analysis on DCs stimulated for 18 h with *L. monocytogenes* ATCC F5817 at MOI = 1. Injections are indicated by dashed vertical lines. $n = 3$. (**E**) Intracellular bacterial replication in DCs incubated for 18 h in antibiotic-free media with and without iNOSib following coincubation with *L. monocytogenes* ATCC 19115 and modified gentamicin protection assay. Analyzed by multiple *t* tests, adjusted *p* values are reported (*p* value > 0.05 ns). $n = 6$, representative of two independent experiments. (**F**) Intracellular bacterial replication in DCs incubated for 18 h in antibiotic-free media with and without iNOSib following coincubation with *L. monocytogenes* ATCC F5817 and modified gentamicin protection assay. Analyzed by multiple *t* tests, adjusted *p* values are reported (*p* value > 0.05 ns). $n = 6$, representative of two independent experiments. 11.2: B6.PWD-Chr11.2; iNOSib, iNOS inhibitor SEITU.

were significantly higher in 11.2 DCs than B6 DCs and not influenced by iNOS inhibition, demonstrating impaired control of this pathogen in 11.2 DCs (Fig. 5D, 5E). Together, these data show that within the context of genetically driven differential regulation of iNOS activity, reducing NO-mediated self-toxicity by virtue of restrained NO production can come at the immunological "price" of reduced innate immune control of bacterial replication.

Discussion

One of the interesting outcomes of these studies was the observation that iNOS regulation occurs at multiple levels between the B6 and PWD DCs. On the full PWD genetic background, iNOS activity is potently regulated at the *Nos2* transcriptional level. In contrast, iNOS induction occurs more readily in LPS-stimulated 11.2 DCs compared with PWD DCs, indicating that PWD alleles outside the 11.2 congenic interval influence transcriptional induction of *Nos2*. In the B6 versus 11.2 DC model, we observed lower NO production at both LPS doses in 11.2 DCs than B6 DCs, even in conditions in which *Nos2* gene transcription and iNOS protein levels were equivalent. This is a provocative finding because it suggests that there are both transcriptional and posttranscriptional differences in the way that NO production is regulated. Importantly, in addition to numerous noncoding SNPs, the PWD *Nos2* allele differs from B6 by six nonsynonymous SNPs. We suspect that these amino acid polymorphisms in *Nos2* likely contribute to differential NO production between B6 and 11.2 DCs, and this is a subject of ongoing work in our laboratory. We speculate that these coding polymorphisms may influence either the dimerization or enzyme kinetics of the iNOS complex, thereby explaining differential NO production, even when total iNOS protein levels are equivalent. In our genetic complementation assay, we saw that the phenotype of higher mitochondrial respiration was preserved in the F1-B6 versus F1-11.2 experiments. These findings suggest that differential NO production between the F1s is at least partially driven by differences in iNOS enzyme activity itself and not differential gene activation. It is not yet fully clear whether differential enzyme activity is strictly the result of the six amino acid polymorphisms in the iNOS gene and/or the result of ∼1000 other genes in the 11.2 interval that could potentially modulate iNOS activity. The most probable explanation is that both structural and regulatory sequence differences in the PWD *Nos2* locus drive functional and expression differences, and a future direction of this work is to evaluate which polymorphisms (if any) drive the phenotype of differential NO production.

iNOS induction is a major topic of discussion when considering how mouse models represent human immunology (50), as LPS stimulation induces high levels of NO production in murine DCs and macrophages that is not replicated in human DC counterparts (moDCs) in vitro. This key difference has led many to believe that murine myeloid cells are poor models for human myeloid cells, but others have built the case that in vitro human DC and macrophage cultures stimulated with LPS plus IFN-γ are poor models for in vivo human DC subsets (50). Although the role of NO is complex and sometimes contradictory, *NOS2* polymorphisms in humans predict susceptibility to numerous infectious diseases (21–24, 51). Additionally, iNOS expression detected in human *Mycobacterium tuberculosis* granulomas indicates that NO production is a component of the innate immune response during infection (5). Taken together, there is evidence that iNOS induction occurs in human DCs but in response to stimuli from environmental signals that have not been fully recapitulated by in vitro models (50). Despite this, there are reported instances of successful generation of in vitro human DCs that make NO (52). In human DCs, low induction of iNOS in response to LPS plus IFN-γ stimulation has been ascribed to higher methylation of the transcriptional start site compared with the mouse (53, 54) as well as to mechanisms of posttranscriptional control (55). In this study, we have described a murine DC model with lower NO production than B6 DCs and have provided initial evidence that multiple levels of regulation (e.g., response to magnitude of activating stimuli,

transcriptional regulation, posttranscriptional/translational regulation, and possible protein sequence/enzyme activity) govern these differences. Therefore, we propose that 11.2 DCs are an improved model of iNOS induction in human DCs, given the restrained nature of NO production on this genetic background.

Recent work in macrophages has demonstrated NO-mediated changes in TCA cycle flux (46–49) through inhibition of enzymes, including pyruvate dehydrogenase, mitochondrial aconitase, and isocitrate dehydrogenase. Activated macrophages also experience inhibition of pyruvate dehydrogenase and α-ketoglutarate dehydrogenase (also known as oxoglutarate dehydrogenase) mediated by changes in lipoylation, which the authors suggest may be modulated by NO production (56). There are many phenotypic similarities between LPS plus IFN-γ–activated macrophages and LPS-stimulated DCs, including increased glycolytic flux and induction of iNOS (8). In activated DCs, it is well established that NO is responsible for impaired electron transport chain function (11, 15), but studies upstream looking at TCA cycle flux have not elucidated mechanisms of reprogramming that occur independently of electron transport chain inhibition. In this study we identify citrate and α-ketoglutarate as metabolites impacted by NO, which is in agreement with findings in the macrophage field. The elucidation of the mechanism(s) of NO-mediated modulation of TCA cycle flux in DCs represents an area of future interest, as there is active debate in the macrophage field as to whether NO-mediated citrate accumulation is driven by inhibition of mitochondrial aconitase or isocitrate dehydrogenase (reviewed in 44).

One of the interesting aspects of NO biology is its role in straddling the balance between antimicrobial activity and self-toxicity, a theme of inflammatory processes in general. We demonstrate in this work that a deficit in NO production, as exhibited in the 11.2 DCs, leads to impaired bacterial killing in our cell culture model. In future studies, we hope to employ our model to study how low NO production mediates other aspects of the DC-dependent immune response (e.g., Ag presentation) rather than studying direct bacterial killing. For example, NO has been shown to modulate inflammatory cytokine production (48). Additionally, we intend to perform follow-up studies in vivo because of contradicting reports that NO aids (57) versus prevents *L. monocytogenes* vacuolar escape (58). In vivo studies may also help elucidate the paracrine effects of various levels of NO production on other immune cells in the immune microenvironment. Overall, this study identifies a new genetic model, whereby restrained NO production can shed insight into NO-mediated immune regulation at both the metabolic and cellular levels.

Acknowledgments

Special acknowledgment goes to Dr. Paula Deming (and the Department of Biomedical and Health Sciences at the University of Vermont [UVM]) and Dr. Ralph Budd (and the UVM Vermont Center for Immunobiology and Infectious Disease Center of Biomedical Research Excellence) for extensive support. Additional acknowledgment goes to the UVM Larner College of Medicine Flow Cytometry and Cell Sorting Facility and for use of the Cytek Aurora from National Institutes of Health S10-ODO026843.

Disclosures

The authors have no financial conflicts of interest.

References

1. Akira, S., and K. Takeda. 2004. Toll-like receptor signalling. *Nat. Rev. Immunol.* 4: 499–511.
2. Amati, L., M. Pepe, M. E. Passeri, M. L. Mastronardi, E. Jirillo, and V. Covelli. 2006. Toll-like receptor signaling mechanisms involved in dendritic cell activation: potential therapeutic control of T cell polarization. *Curr. Pharm. Des.* 12: 4247–4254.
3. Barton, G. M., and R. Medzhitov. 2002. Control of adaptive immune responses by Toll-like receptors. *Curr. Opin. Immunol.* 14: 380–383.
4. Banchereau, J., and R. M. Steinman. 1998. Dendritic cells and the control of immunity. *Nature* 392: 245–252.
5. Mattila, J. T., O. O. Ojo, D. Kepka-Lenhart, S. Marino, J. H. Kim, S. Y. Eum, L. E. Via, C. E. Barry III, E. Klein, D. E. Kirschner, et al. 2013. Microenvironments in tuberculous granulomas are delineated by distinct populations of macrophage subsets and expression of nitric oxide synthase and arginase isoforms. *J. Immunol.* 191: 773–784.
6. Chapman, N. M., M. R. Boothby, and H. Chi. 2020. Metabolic coordination of T cell quiescence and activation. *Nat. Rev. Immunol.* 20: 55–70.
7. Sandoval, H., S. Kodali, and J. Wang. 2018. Regulation of B cell fate, survival, and function by mitochondria and autophagy. *Mitochondrion* 41: 58–65.
8. van Teijlingen Bakker, N., and E. J. Pearce. 2020. Cell-intrinsic metabolic regulation of mononuclear phagocyte activation: findings from the tip of the iceberg. *Immunol. Rev.* 295: 54–67.
9. Chang, C. H., J. D. Curtis, L. B. Maggi, Jr., B. Faubert, A. V. Villarino, D. O'Sullivan, S. C. Huang, G. J. van der Windt, J. Blagih, J. Qiu, et al. 2013. Posttranscriptional control of T cell effector function by aerobic glycolysis. *Cell* 153: 1239–1251.
10. Everts, B., E. Amiel, S. C. Huang, A. M. Smith, C. H. Chang, W. Y. Lam, V. Redmann, T. C. Freitas, J. Blagih, G. J. van der Windt, et al. 2014. TLR-driven early glycolytic reprogramming via the kinases TBK1-IKKε supports the anabolic demands of dendritic cell activation. *Nat. Immunol.* 15: 323–332.
11. Everts, B., E. Amiel, G. J. van der Windt, T. C. Freitas, R. Chott, K. E. Yarasheski, E. L. Pearce, and E. J. Pearce. 2012. Commitment to glycolysis sustains survival of NO-producing inflammatory dendritic cells. *Blood* 120: 1422–1431.
12. Krawczyk, C. M., T. Holowka, J. Sun, J. Blagih, E. Amiel, R. J. DeBerardinis, J. R. Cross, E. Jung, C. B. Thompson, R. G. Jones, and E. J. Pearce. 2010. Toll-like receptor-induced changes in glycolytic metabolism regulate dendritic cell activation. *Blood* 115: 4742–4749.
13. van der Windt, G. J., D. O'Sullivan, B. Everts, S. C. Huang, M. D. Buck, J. D. Curtis, C. H. Chang, A. M. Smith, T. Ai, B. Faubert, et al. 2013. CD8 memory T cells have a bioenergetic advantage that underlies their rapid recall ability. *Proc. Natl. Acad. Sci. USA* 110: 14336–14341.
14. Amiel, E., B. Everts, T. C. Freitas, I. L. King, J. D. Curtis, E. L. Pearce, and E. J. Pearce. 2012. Inhibition of mechanistic target of rapamycin promotes dendritic cell activation and enhances therapeutic autologous vaccination in mice. *J. Immunol.* 189: 2151–2158.
15. Amiel, E., B. Everts, D. Fritz, S. Beauchamp, B. Ge, E. L. Pearce, and E. J. Pearce. 2014. Mechanistic target of rapamycin inhibition extends cellular lifespan in dendritic cells by preserving mitochondrial function. *J. Immunol.* 193: 2821–2830.
16. Harris, A. J., A. R. Thompson, M. K. Whyte, and S. R. Walmsley. 2014. HIF-mediated innate immune responses: cell signaling and therapeutic implications. *Hypoxia (Auckl.)* 2: 47–58.
17. Lawless, S. J., N. Kedia-Mehta, J. F. Walls, R. McGarrigle, O. Convery, L. V. Sinclair, M. N. Navarro, J. Murray, and D. K. Finlay. 2017. Glucose represses dendritic cell-induced T cell responses. *Nat. Commun.* 8: 15620.
18. Barone, M. C., V. M. Darley-Usmar, and P. S. Brookes. 2003. Reversible inhibition of cytochrome c oxidase by peroxynitrite proceeds through ascorbate-dependent generation of nitric oxide. *J. Biol. Chem.* 278: 27520–27524.
19. Clementi, E., G. C. Brown, M. Feelisch, and S. Moncada. 1998. Persistent inhibition of cell respiration by nitric oxide: crucial role of S-nitrosylation of mitochondrial complex I and protective action of glutathione. *Proc. Natl. Acad. Sci. USA* 95: 7631–7636.
20. Thwe, P. M., L. R. Pelgrom, R. Cooper, S. Beauchamp, J. A. Reisz, A. D'Alessandro, B. Everts, and E. Amiel. 2017. Cell-intrinsic glycogen metabolism supports early glycolytic reprogramming required for dendritic cell immune responses. [Published erratum appears in 2019 *Cell Metab.* 30: 225.] *Cell Metab.* 26: 558–567.e5.
21. Gómez, L. M., J. M. Anaya, J. R. Vilchez, J. Cadena, R. Hinojosa, L. Vélez, M. A. Lopez-Nevot, and J. Martín. 2007. A polymorphism in the inducible nitric oxide synthase gene is associated with tuberculosis. *Tuberculosis (Edinb.)* 87: 288–294.
22. Hobbs, M. R., V. Udhayakumar, M. C. Levesque, J. Booth, J. M. Roberts, A. N. Tkachuk, A. Pole, H. Coon, S. Kariuki, B. L. Nahlen, et al. 2002. A new NOS2 promoter polymorphism associated with increased nitric oxide production and protection from severe malaria in Tanzanian and Kenyan children. *Lancet* 360: 1468–1475.
23. Kun, J. F., B. Mordmüller, D. J. Perkins, J. May, O. Mercereau-Puijalon, M. Alpers, J. B. Weinberg, and P. G. Kremsner. 2001. Nitric oxide synthase 2(Lambaréné) (G-954C), increased nitric oxide production, and protection against malaria. *J. Infect. Dis.* 184: 330–336.
24. Levesque, M. C., M. R. Hobbs, C. W. O'Loughlin, J. A. Chancellor, Y. Chen, A. N. Tkachuk, J. Booth, K. B. Patch, S. Allgood, A. R. Pole, et al. 2010. Malaria severity and human nitric oxide synthase type 2 (NOS2) promoter haplotypes. *Hum. Genet.* 127: 163–182.
25. Liu, J. J., H. Duan, and S. Wang. 2013. [Expression of nitric oxide in uterine junctional zone of patients with adenomyosis]. *Zhonghua Fu Chan Ke Za Zhi* 48: 504–507.
26. Jia, T., N. V. Serbina, K. Brandl, M. X. Zhong, I. M. Leiner, I. F. Charo, and E. G. Pamer. 2008. Additive roles for MCP-1 and MCP-3 in CCR2-mediated recruitment of inflammatory monocytes during *Listeria monocytogenes* infection. *J. Immunol.* 180: 6846–6853.

27. Serbina, N. V., T. P. Salazar-Mather, C. A. Biron, W. A. Kuziel, and E. G. Pamer. 2003. TNF/iNOS-producing dendritic cells mediate innate immune defense against bacterial infection. *Immunity* 19: 59–70.
28. Pacher, P., J. S. Beckman, and L. Liaudet. 2007. Nitric oxide and peroxynitrite in health and disease. *Physiol. Rev.* 87: 315–424.
29. Zwaferink, H., S. Stockinger, S. Reipert, and T. Decker. 2008. Stimulation of inducible nitric oxide synthase expression by beta interferon increases necrotic death of macrophages upon *Listeria monocytogenes* infection. *Infect. Immun.* 76: 1649–1656.
30. Thwe, P. M., and E. Amiel. 2018. The role of nitric oxide in metabolic regulation of dendritic cell immune function. *Cancer Lett.* 412: 236–242.
31. Bearoff, F., R. Del Rio, L. K. Case, J. A. Dragon, T. Nguyen-Vu, C. Y. Lin, E. P. Blankenhorn, C. Teuscher, and D. N. Krementsov. 2016. Natural genetic variation profoundly regulates gene expression in immune cells and dictates susceptibility to CNS autoimmunity. *Genes Immun.* 17: 386–395.
32. Dupont, M. S. J., V. Guillemot, P. Campagne, N. Serafini, S. Marie, X. Montagutelli, J. P. Di Santo, and C. A. J. Vosshenrich. 2021. Host genetic control of natural killer cell diversity revealed in the Collaborative Cross. *Proc. Natl. Acad. Sci. USA* 118: e2018834118.
33. Graham, J. B., J. L. Swarts, M. Mooney, G. Choonoo, S. Jeng, D. R. Miller, M. T. Ferris, S. McWeeney, and J. M. Lund. 2017. Extensive Homeostatic T Cell Phenotypic Variation within the Collaborative Cross. *Cell Rep.* 21: 2313–2325.
34. Krementsov, D. N., L. Asarian, Q. Fang, M. M. McGill, and C. Teuscher. 2018. Sex-specific gene-by-vitamin D interactions regulate susceptibility to central nervous system autoimmunity. *Front. Immunol.* 9: 1622.
35. Lahue, K. G., M. K. Lara, A. A. Linton, B. Lavoie, Q. Fang, M. M. McGill, J. W. Crothers, C. Teuscher, G. M. Mawe, A. L. Tyler, et al. 2020. Identification of novel loci controlling inflammatory bowel disease susceptibility utilizing the genetic diversity of wild-derived mice. *Genes Immun.* 21: 311–325.
36. Phillippi, J., Y. Xie, D. R. Miller, T. A. Bell, Z. Zhang, A. B. Lenarcic, D. L. Aylor, S. H. Krovi, D. W. Threadgill, F. P. de Villena, et al. 2014. Using the emerging Collaborative Cross to probe the immune system. *Genes Immun.* 15: 38–46.
37. Gregorová, S., and J. Forejt. 2000. PWD/Ph and PWK/Ph inbred mouse strains of *Mus* m. musculus subspecies–a valuable resource of phenotypic variations and genomic polymorphisms. *Folia Biol. (Praha)* 46: 31–41.
38. Guak, H., S. Al Habyan, E. H. Ma, H. Aldossary, M. Al-Masri, S. Y. Won, T. Ying, E. D. Fixman, R. G. Jones, L. M. McCaffrey, and C. M. Krawczyk. 2018. Glycolytic metabolism is essential for CCR7 oligomerization and dendritic cell migration. *Nat. Commun.* 9: 2463.
39. Raza, A., J. W. Crothers, M. M. McGill, G. M. Mawe, C. Teuscher, and D. N. Krementsov. 2017. Anti-inflammatory roles of p38α MAPK in macrophages are context dependent and require IL-10. *J. Leukoc. Biol.* 102: 1219–1227.
40. Bertolone, L., H. K. Shin, D. Stefanoni, J. H. Baek, Y. Gao, E. J. Morrison, T. Nemkov, T. Thomas, R. O. Francis, E. A. Hod, et al. 2020. ZOOMICS: comparative metabolomics of red blood cells from old world monkeys and humans. *Front. Physiol.* 11: 593841.
41. Catala, A., L. A. Youssef, J. A. Reisz, M. Dzieciatkowska, N. E. Powers, C. Marchetti, M. Karafin, J. C. Zimring, K. E. Hudson, K. C. Hansen, et al. 2020. metabolic reprogramming of mouse bone marrow derived macrophages following erythrophagocytosis. *Front. Physiol.* 11: 396.
42. Adams, D. J., A. G. Doran, J. Lilue, and T. M. Keane. 2015. The Mouse Genomes Project: a repository of inbred laboratory mouse strain genomes. *Mamm. Genome* 26: 403–412.
43. Montgomery, T. L., A. Künstner, J. J. Kennedy, Q. Fang, L. Asarian, R. Culp-Hill, A. D'Alessandro, C. Teuscher, H. Busch, and D. N. Krementsov. 2020. Interactions between host genetics and gut microbiota determine susceptibility to CNS autoimmunity. *Proc. Natl. Acad. Sci. USA* 117: 27516–27527.
44. Jansa, P., P. Divina, and J. Forejt. 2005. Construction and characterization of a genomic BAC library for the *Mus* m. musculus mouse subspecies (PWD/Ph inbred strain). *BMC Genomics* 6: 161.
45. Gregorová, S., P. Divina, R. Storchova, Z. Trachtulec, V. Fotopulosova, K. L. Svenson, L. R. Donahue, B. Paigen, and J. Forejt. 2008. Mouse consomic strains: exploiting genetic divergence between *Mus* m. musculus and *Mus* m. domesticus subspecies. *Genome Res.* 18: 509–515.
46. Palmieri, E. M., C. McGinity, D. A. Wink, and D. W. McVicar. 2020. Nitric oxide in macrophage immunometabolism: hiding in plain sight. *Metabolites* 10: 429.
47. Somasundaram, A., N. J. Rothenberger, and L. P. Stabile. 2020. The impact of estrogen in the tumor microenvironment. *Adv. Exp. Med. Biol.* 1277: 33–52.
48. Bailey, J. D., M. Diotallevi, T. Nicol, E. McNeill, A. Shaw, S. Chuaiphichai, A. Hale, A. Starr, M. Nandi, E. Stylianou, et al. 2019. Nitric oxide modulates metabolic remodeling in inflammatory macrophages through TCA cycle regulation and itaconate accumulation. *Cell Rep.* 28: 218–230.e7.
49. Palmieri, E. M., M. Gonzalez-Cotto, W. A. Baseler, L. C. Davies, B. Ghesquière, N. Maio, C. M. Rice, T. A. Rouault, T. Cassel, R. M. Higashi, et al. 2020. Nitric oxide orchestrates metabolic rewiring in M1 macrophages by targeting aconitase 2 and pyruvate dehydrogenase. *Nat. Commun.* 11: 698.
50. Thomas, A. C., and J. T. Mattila. 2014. "Of mice and men": arginine metabolism in macrophages. *Front. Immunol.* 5: 479.
51. Wang, Z., K. Feng, M. Yue, X. Lu, Q. Zheng, H. Zhang, Y. Zhai, P. Li, L. Yu, M. Cai, et al. 2013. A non-synonymous SNP in the NOS2 associated with septic shock in patients with sepsis in Chinese populations. *Hum. Genet.* 132: 337–346.
52. Wilsmann-Theis, D., S. Koch, C. Mindnich, S. Bonness, S. Schnautz, D. von Bubnoff, and T. Bieber. 2013. Generation and functional analysis of human TNF-α/iNOS-producing dendritic cells (Tip-DC). *Allergy* 68: 890–898.
53. Gross, T. J., K. Kremens, L. S. Powers, B. Brink, T. Knutson, F. E. Domann, R. A. Philibert, M. M. Milhem, and M. M. Monick. 2014. Epigenetic silencing of the human NOS2 gene: rethinking the role of nitric oxide in human macrophage inflammatory responses. *J. Immunol.* 192: 2326–2338.
54. Zhang, X., V. E. Laubach, E. W. Alley, K. A. Edwards, P. A. Sherman, S. W. Russell, and W. J. Murphy. 1996. Transcriptional basis for hyporesponsiveness of the human inducible nitric oxide synthase gene to lipopolysaccharide/interferon-gamma. *J. Leukoc. Biol.* 59: 575–585.
55. Pautz, A., J. Art, S. Hahn, S. Nowag, C. Voss, and H. Kleinert. 2010. Regulation of the expression of inducible nitric oxide synthase. *Nitric Oxide* 23: 75–93.
56. Seim, G. L., E. C. Britt, S. V. John, F. J. Yeo, A. R. Johnson, R. S. Eisenstein, D. J. Pagliarini, and J. Fan. 2019. Two-stage metabolic remodelling in macrophages in response to lipopolysaccharide and interferon-γ stimulation. *Nat. Metab.* 1: 731–742.
57. Cole, C., S. Thomas, H. Filak, P. M. Henson, and L. L. Lenz. 2012. Nitric oxide increases susceptibility of Toll-like receptor-activated macrophages to spreading *Listeria monocytogenes*. *Immunity* 36: 807–820.
58. Myers, J. T., A. W. Tsang, and J. A. Swanson. 2003. Localized reactive oxygen and nitrogen intermediates inhibit escape of *Listeria monocytogenes* from vacuoles in activated macrophages. *J. Immunol.* 171: 5447–5453.